CHAPTER 9

STUDY OF THE ROLE OF SMALL MOLECULE INHIBITOR IN PREVENTING AGGREGATION OF α-SYNUCLEIN

Study of the role of small molecule inhibitor in preventing aggregation of α-Synuclein

9.1. Abstract:

PD is characterized by distinct aggregated fibrillary form of αS known as the Lewy bodies and Lewy neurites. The most promising approach to combat PD is to prevent the misfolding and subsequent aggregation of αS. Recently, Oleuropein aglycone (OleA) has been reported to stabilize the monomeric structure of αS, subsequently favoring the growth of non-toxic aggregates. Therefore, understanding the conformational dynamics of αS monomer in presence of OleA is significant. Here, we have investigated the effect of OleA on the conformational dynamics and the aggregation propensity of αS using molecular dynamics simulation. From MD trajectory analysis, we noticed that when OleA is bound to αS, the intra-molecular distance between non-amyloid-β component (NAC) domain and C-terminal domain of αS was increased, while long-range hydrophobic interactions between the two region was reduced. OleA was found to interact with the N-terminal domain of αS, making this region unavailable for interaction with membranes and lipids for the formation of cellular toxic aggregates. From the binding free energy (BFE) analysis, we found binding affinity between αS and OleA to be indeed high (ΔG_{bind} = -12.56 kcal mol^{-1} from MM-PBSA and ΔG_{bind} = -27.41 kcal mol^{-1} from MM-GBSA). Our findings in this study thus substantiate the effect of OleA on the structure and stabilization of αS monomer that subsequently favors growth of stable and non-toxic aggregates.

9.2. Introduction:

The exact cure for PD has been a bigger arena of research in the drug and pharmaceutical industry. There has always been a hunt for natural molecules, which would prevent αS oligomerization, fibrillation and thus the potential to reduce the toxicity of preformed aggregated species. Many small organic, as well as inorganic molecules have been reported to behave as the potential therapeutic agents for the treatment of PD [670, 671]. The search for small molecules having the potential to inhibit the interaction of aggregated αS with the membrane, reduction of formation of reactive oxygen species (ROS), and decreasing the level of formation of Ca^{2+} in the cytoplasm, has proven to be challenging.

Recent studies have shown the potential of flavonoids and polyphenolic compounds to play an important role in the cure of PD and other neurodegenerative disorders [672, 673]. One such phenolic compound is Oleuropein aglycone (OleA), a secoiridoid obtained from olive cultivars, which has been reported to have an anti-aggregation effect on the αS protein. Olive's polyphenolic compounds have been known to possess many medicinal properties, such as neuroprotection, anti-inflammatory, and antioxidant properties. However, only a few studies have been carried out to understand the role of OleA in the aggregation propensity of αS [624, 674]. A new study reported that OleA interferes with the aggregation mechanism in vitro of several peptides/proteins associated with amyloid diseases including amylin, Aβ peptides, tau, transthyretin, and beta2-microglobulin [674]. A recent study has highlighted that OleA stabilizes the monomeric αS and favors the growth of non-toxic aggregates [674]. However, the role of OleA on the conformational changes in the monomeric structure of αS at the molecular level is not well studied. Therefore, in this computational work, we have used molecular dynamics (MD) simulations to demonstrate the effect of OleA on the structure and stabilisation of αS monomer that subsequently favours the growth of stable and non-toxic aggregates [675].

9.3. Materials and methods

9.3.1. Molecular docking and the preparation of initial structures

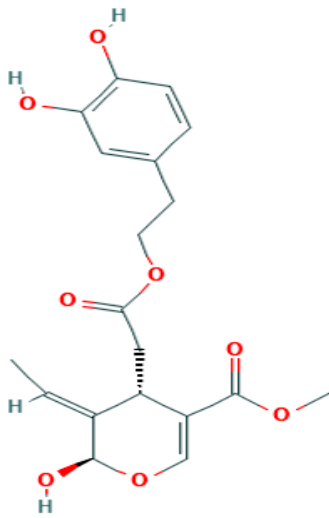### 9.3.1.1. Preparation of receptor:

The micelle-bound human αS monomeric structure, PDB ID: 1XQ8 [275] obtained from RCSB Protein Data Bank [502, 503] was used as the receptor molecule for molecular docking.

9.3.1.2. Preparation of ligand:

The structure of OleA (ligand) in SDF format (PubChem CID: 56842347) was taken from PubChem online server [620]. The SDF format of OleA structure was then changed to PDB format using Open Bable server [621]. The physico-chemical properties of OleA were summarized in **Table 9.1**.

*Table 9.1.* *Physico-chemical properties of Oleuropein aglycone (OleA)*

Chemical structure	
Chemical name) (IUPAC	methyl (2R,3E,4S)-4-{2-[2-(3,4-dihydroxyphenyl)ethoxy]-2-oxoethyl}-3-ethylidene-2-hydroxy-3,4-dihydro-2H-pyran-5-carboxylate
SMILES	COC(=O)C1=COC(C(=CC)C1CC(=O)OCCc1ccc(c(c1)O)O)O
Molecular formula	$C_{19}H_{22}O_8$
Molecular weight	378.377 g/mol
H-Bond donor	8
H-Bond acceptor	3
Log P^c	1.34
Rotatable bonds	8
TPSA (A^2)	122.53

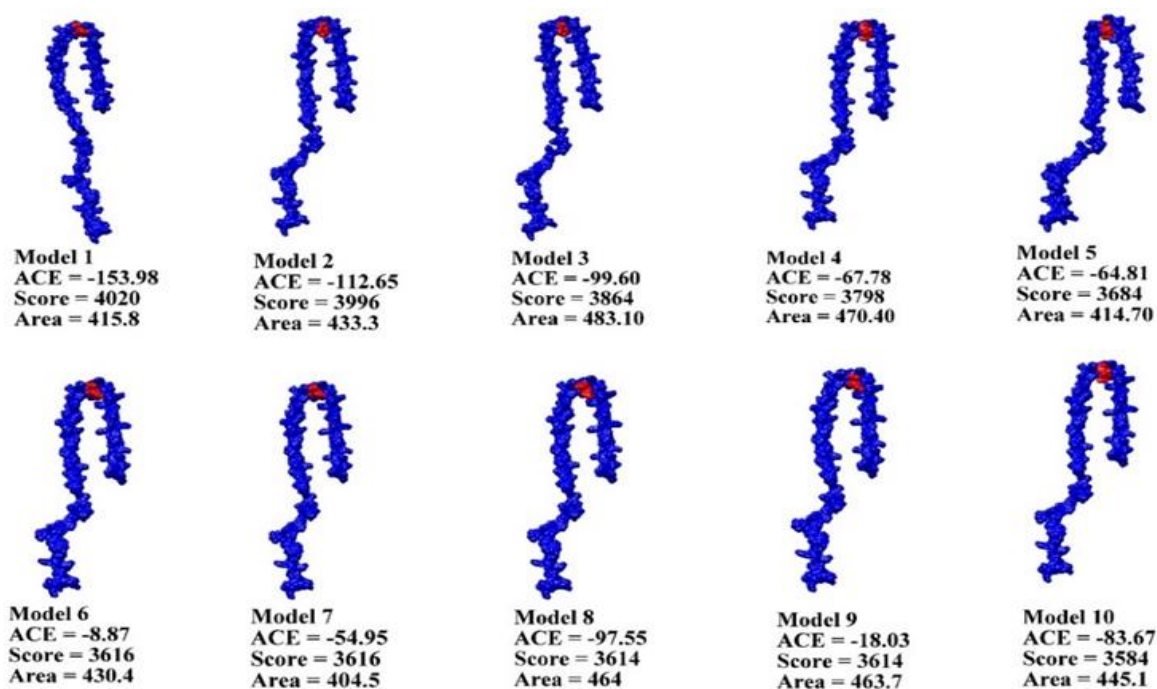TPSA = Topological polar surface area; logP = octanol-water partition coefficients

9.3.1.3. Preparation of the complex:

The receptor molecule (αS) retrieved from Protein Data Bank was then docked to the ligand (OleA) using the Patchdock [511], an online docking server. The schematic representation of preparation of complex from receptor molecule and ligand molecule is shown in **Figure 9.1**. From the many resulting docked complexes (**Figure 9.2**) obtained from Patchdock server, the one with the highest atomic contact energy (ACE), geometric surface, and the geometric shape complementarity score, was selected as the initial complex structure (**Model 1** from **Figure 9.2**) in this study. This complex structure was viewed, the ligand and receptor portions of the complex were then separated and their co-ordinates were saved in mol2 and PDB format respectively using UCSF Chimera package alpha v.1.12 [530]. The selected solution structure was further curated in xleap using antechamber protocol (as mentioned in *section 6.3.1.3*). We have carried out the MD simulations on the complex system using explicit solvation. However, for the binding free energy analysis, the required topology and parameter input files were also

prepared. We have also carried out two other additional MD simulations in this study with Model 2 and Model 3 (**Figure 9.2**) as initial complex structure respectively. These complex structures differ in atomic contact energy (ACE), geometric surface, and the geometric shape complementarity score.
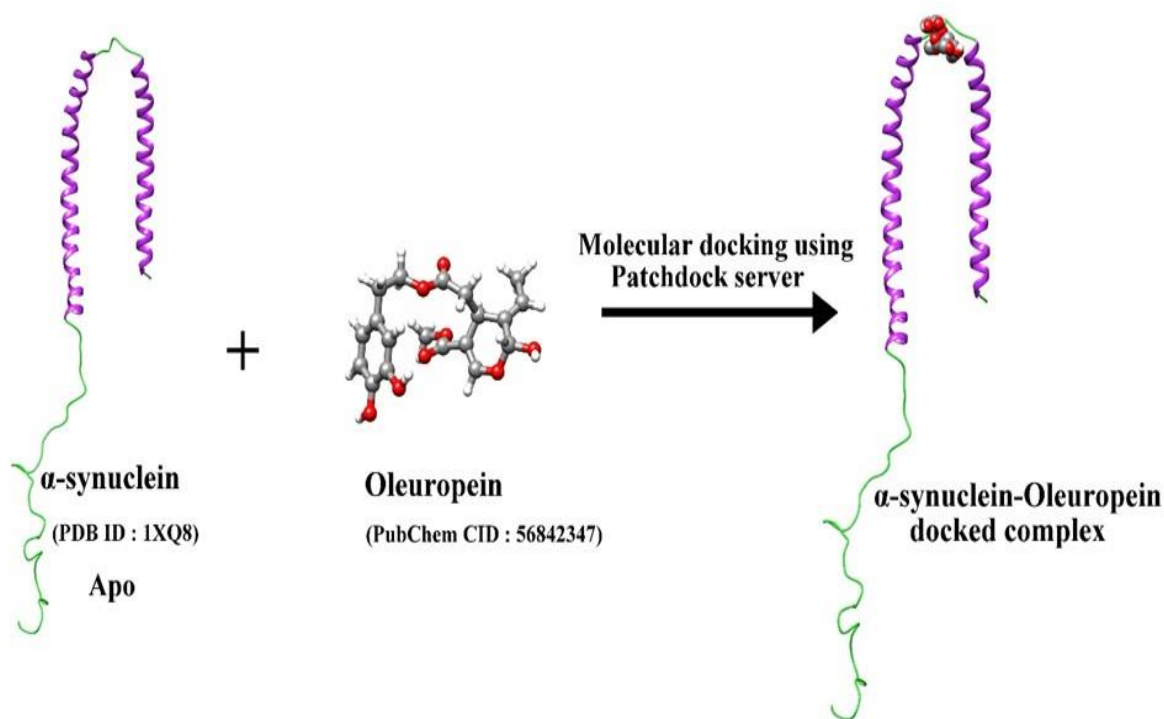
Figure 9.1. Schematic representation showing the formation of docked complex from α-Synuclein (PDB ID-1XQ8) and Oleuropein aglycone (OleA).

Model 1
ACE = -153.98
Score = 4020
Area = 415.8

Model 2
ACE = -112.65
Score = 3996
Area = 433.3

Model 3
ACE = -99.60
Score = 3864
Area = 483.10

Model 4
ACE = -67.78
Score = 3798
Area = 470.40

Model 5
ACE = -64.81
Score = 3684
Area = 414.70

Model 6
ACE = -8.87
Score = 3616
Area = 430.4

Model 7
ACE = -54.95
Score = 3616
Area = 404.5

Model 8
ACE = -97.55
Score = 3614
Area = 464

Model 9
ACE = -18.03
Score = 3614
Area = 463.7

Model 10
ACE = -83.67
Score = 3584
Area = 445.1

Figure 9.2. Top 10 representative docked models for (α-Synuclein + OleA) complex generated by Patchdock along with their rankings based on their Atomic Contact Energies (ACE), score and area.

## 9.3.2. Setup for MD simulations:

α-Synuclein monomer (apo) and (α-Synuclein + OleA) complex systems were prepared for the simulation using the AMBER ff99SBildn force field [667, 668] in the Leap module of the AMBER 14 software package. Recent studies have shown that structural ensembles of intrinsically disordered proteins (IDPs) strongly depend on their force field [669]. The rugged energy landscapes of IDPs are highly sensitive test systems capable of revealing force field deficiencies and therefore contributing to force field development. We observed that there is no perfect force field to study IDPs. But available literature shows that ff99SBildn and ff99SB force field have been used in many studies to characterize the salient structural features of IDP [588, 589, 667, 678]. Also, ff99SBildn is the advanced force field of ff99SB for IDP. Hence, we have used ff99SBildn force field to carry out this particular study. Both the α-Synuclein monomer (apo) and (α-Synuclein+ OleA) complex systems were subjected to MD simulation for 50 ns according to the MD simulation steps as discussed in *Section 4.3.2.*

The MD trajectories for both the apo and complex were analyzed using PTRAJ (short for Process TRAJectory) and CPPTRAJ (a rewrite of PTRAJ in C++) module [549] of AmberTools 14. To assess the convergence of our systems, the RMSDs for apo and complex systems were studied, wherein the starting structure of MD was used as the reference. In addition, the convergence of molecular dynamics simulations of the apo and complex structure were also assessed using block average root-mean-square distance method [676]. In this method, the MD trajectory of both apo and complex has been divided into contiguous blocks after aligning the trajectory to the corresponding reference average structure. Then, the average structure for each block and the RMSD between each average structure was computed. The average RMSD value and the standard deviation of RMSD values at each block size are then plotted as a function of block size.

In addition, R_g, SASA, hydrophobic contacts, and intra-molecular distance analysis were carried out for the two systems. The intra-molecular hydrogen bond analysis was employed for NAC and C-terminal region of apo and complex separately based on the potential donors (HD) and acceptors (HA) of the hydrogen atom. For the visualization of the 3D structure of the molecules, UCSF Chimera [530] was used. The xmgrace plotting tools have been used for generating the graphs. To verify the

correctness of the NPT simulation algorithm, the pressure, temperature, potential energy, kinetic energy and total energy of the (α-Synuclein + OleA) complex was plotted as a function of simulation time period (as shown in **Figure 9.3.**)
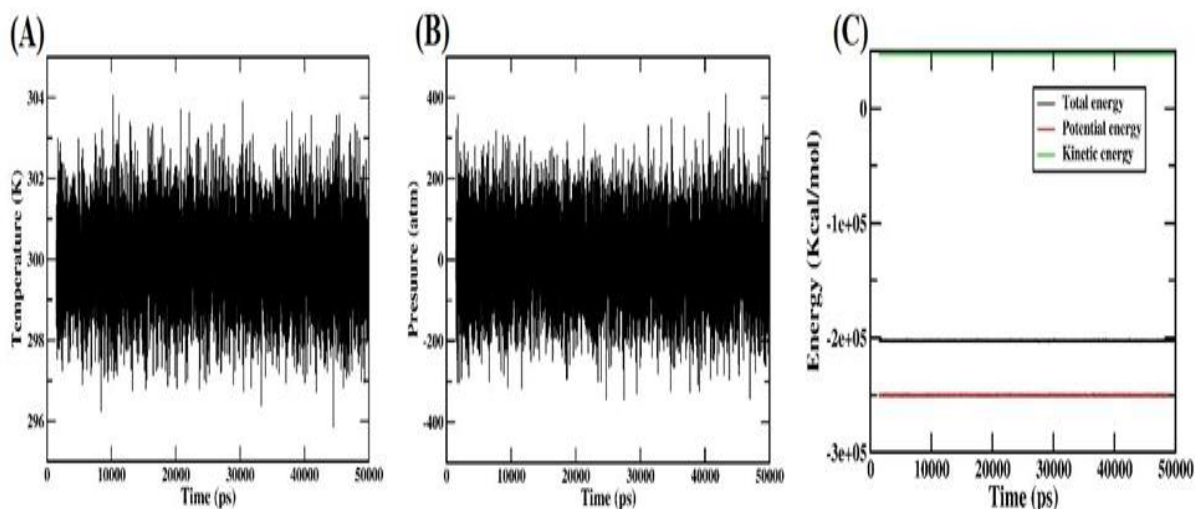
Figure 9.3. *(A) Temperature, (B) Pressure, and (C) Energy plots of (α-Synuclein + OleA) complex system as a function of simulation time.*

9.3.3. MM-PBSA/ GBSA Binding free energy calculation:

The binding free energy (BFE) and the per-residue energy decomposition (PRED) analysis for the (α-Synuclein + OleA) complex were carried out using MMPBSA.py script of the AMBER 14 suite as discussed in *Section 3.1.3.*

9.4. Results and Discussion

9.4.1 Conformational analysis of α-Synuclein (apo) and (α-Synuclein + OleA) complex:

The conformational changes in α-Synuclein (apo) and in the (α-Synuclein + OleA) complex as a function of time were studied using the corresponding 50 ns MD trajectory files. All the preliminary analysis such as root mean square deviation (RMSD), solvent accessible surface area (SASA), Radius of gyration (R_g) plots, B-factor values, and secondary structure analysis have been carried out to ensure the quality of the simulations.

9.4.1.1. Root Mean Square Deviation (RMSD) analysis:

The RMSD values of all Cα-atoms referenced to their starting structures for the

two systems: (a) α-Synuclein (apo) and (b) (α-Synuclein + OleA) complex were determined to assess their stability. The RMSD plots for the complex and apo structure of αS have been depicted in **Figure 9.4(A)**. From the RMSD plot, we observed that the conformation of αS was stable in both apo and in the complex form. In the apo form, the RMSD value was found to oscillate until 21 ns of the simulation period and then converges thereafter at around 7.2 Å. However, in the complex form, the RMSD value shows fluctuation initially and then found to converge around 14.4 Å after 20 ns of the simulation period. We have assessed the convergence of the apo (**Figure 9.5**) and complex structure (**Figure 9.6**) being modeled in our study using block average root-mean-square distance method [676]. From **Figures 9.5(A)** and **9.5(B)**, in the case of apo, we observed that the average RMSD of the trajectory blocks converges at around 7.2 Å and the standard deviation for the RMSD at each block size converges around 0.15 Å after 21 ns. In case of complex, we noticed that the average RMSD of the trajectory blocks converges at around 14.4 Å (**Figure 9.6(A)**) and the standard deviation for the RMSD at each block size converges around 0.25 Å after 20 ns (**Figure 9.6(B)**).

9.4.1.2. Radius of gyration $_{(R_g)}$ analysis:

R_g is usually calculated to estimate the overall dispersion of atoms of a particular biomolecule from their common center of gravity/axis. R_g is an indicator of protein structure's compactness [624]. The R_g values of the apo and complex systems have been depicted in **Figure 9.4(B)**. From the R_g plot, we see that the R_g values for the apo structure was found to converge at around 38.68 Å, while the R_g for the complex structure showed more fluctuation and it ranges from 42-48 Å. From the R_g analysis, we can infer that the αS monomeric structure is more compact in the case of apo form while in the complex form, the monomeric structure of αS adopts a different type of folding at different intervals of the simulation period. Besides, the changes we have seen in the R_g values are the reflections endured by the varied conformations of αS structure and their molecular interactions during the course of the simulation.

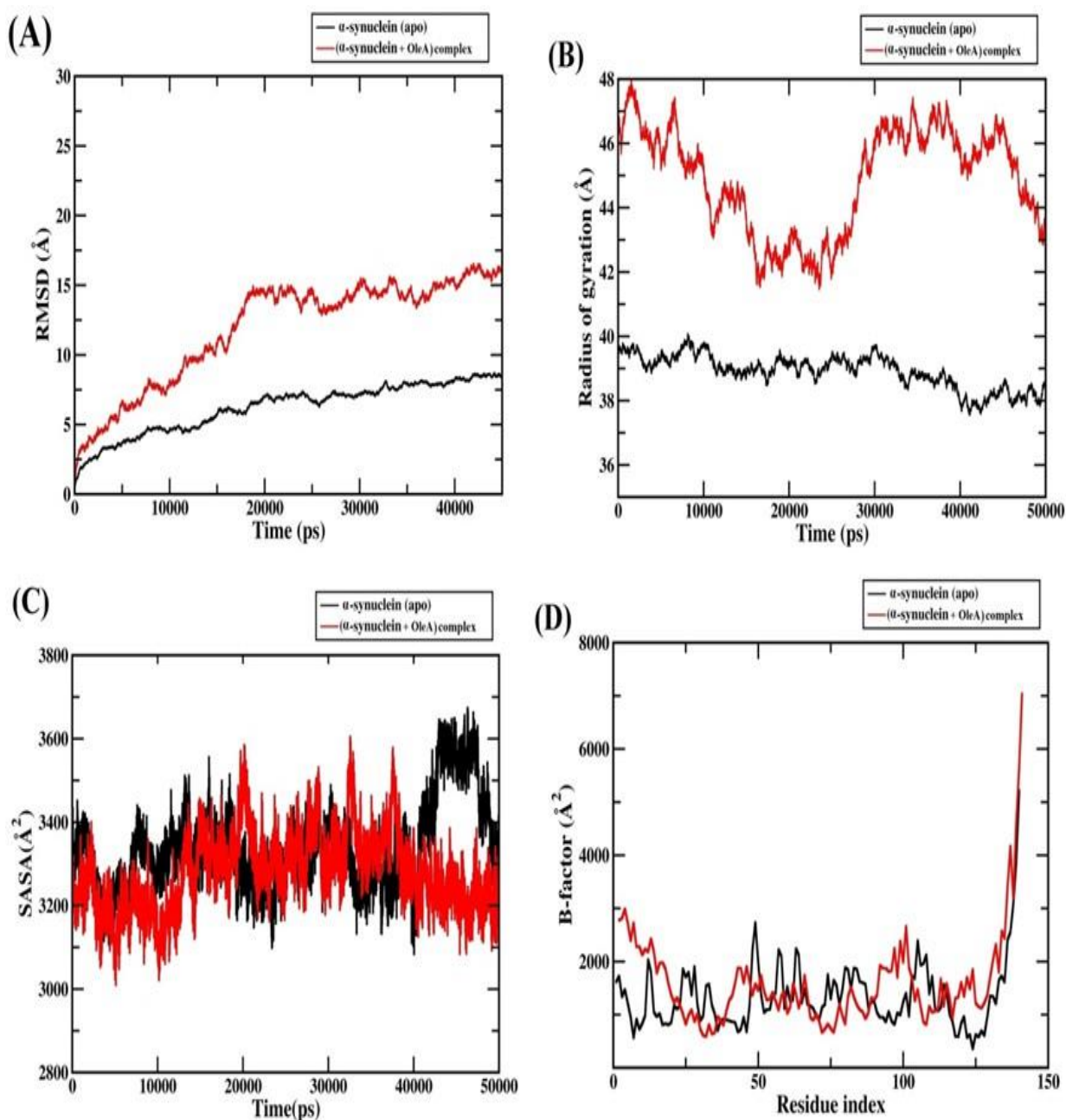## 9.4.1.3. Solvent Accessible Surface Area (SASA) analysis:

The non-amyloid-β component (NAC) region of monomeric αS between residues aa61-95 is the most hydrophobic central region. It folds into a β-sheet structure and plays a critical role in both the aggregation and cytotoxicity [677]. Therefore, it is important to

determine the SASA for the NAC region as it may provide insights into the aggregation propensity of αS. To map out the surface area accessible by the water solvent for our explicit systems, we used a molecular probe of radius 1.4 Å. The NAC region for the apo state ranges from residues aa61-95 while in the complex state it ranges from residues aa62-96. The SASA profile of the NAC region of the apo and complex systems have been shown in **Figure 9.4(C)**. From **Figure 9.4(C)**, we observe the overall SASA for the NAC region in the (α-Synuclein + OleA) complex is quite more than in the α-Synuclein (apo). As a result, we can expect the monomeric structure of αS complexed with OleA to undergo aggregation with greater propensity than the αS monomeric structure in apo form.

9.4.1.4. B-factor analysis:

To analyze the local deformability for the Cα atoms in the apo and complex form of αS, we analyzed B-factor that provides information about the spatial fluctuations of atoms around the equilibrium position. The B-factor values obtained for the backbone Cα atoms in apo and complex forms of αS were computed from the corresponding MD simulation trajectories and were plotted against their residue numbers. From **Figure 9.4(D)**, we observe the Cα atoms atoms in the region corresponding to the N-terminal and NAC domain experiences slightly higher fluctuation in the apo form of αS than in the complex. Therefore we infer that the N-terminal and NAC domain is more flexible in apo form of αS than in the complex.

Figure 9.4. *Comparative Molecular Dynamics analysis of (A) Root mean square deviation, (B) Radius of gyration, (C) Solvent accessible surface area, and (D) B-factor for α-Synuclein (apo), and (α-Synuclein + OleA) complex.*
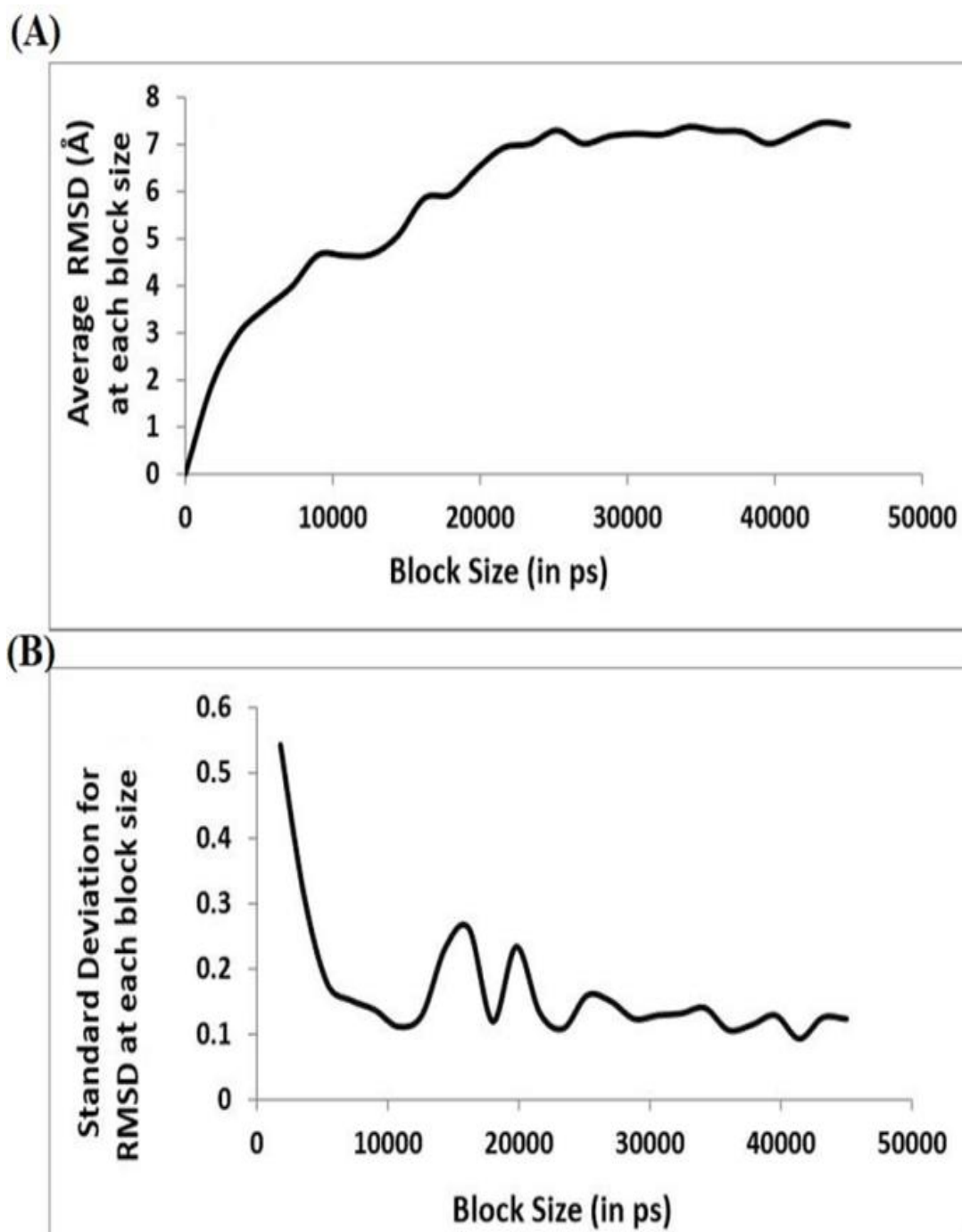
Figure 9.5. *(A) Average RMSD at each block versus block size in picoseconds, (B) Standard deviation for the RMSD at each block size versus block size in picoseconds for the α-Synuclein (apo) Molecular dynamics trajectory.*

(A)

(B)
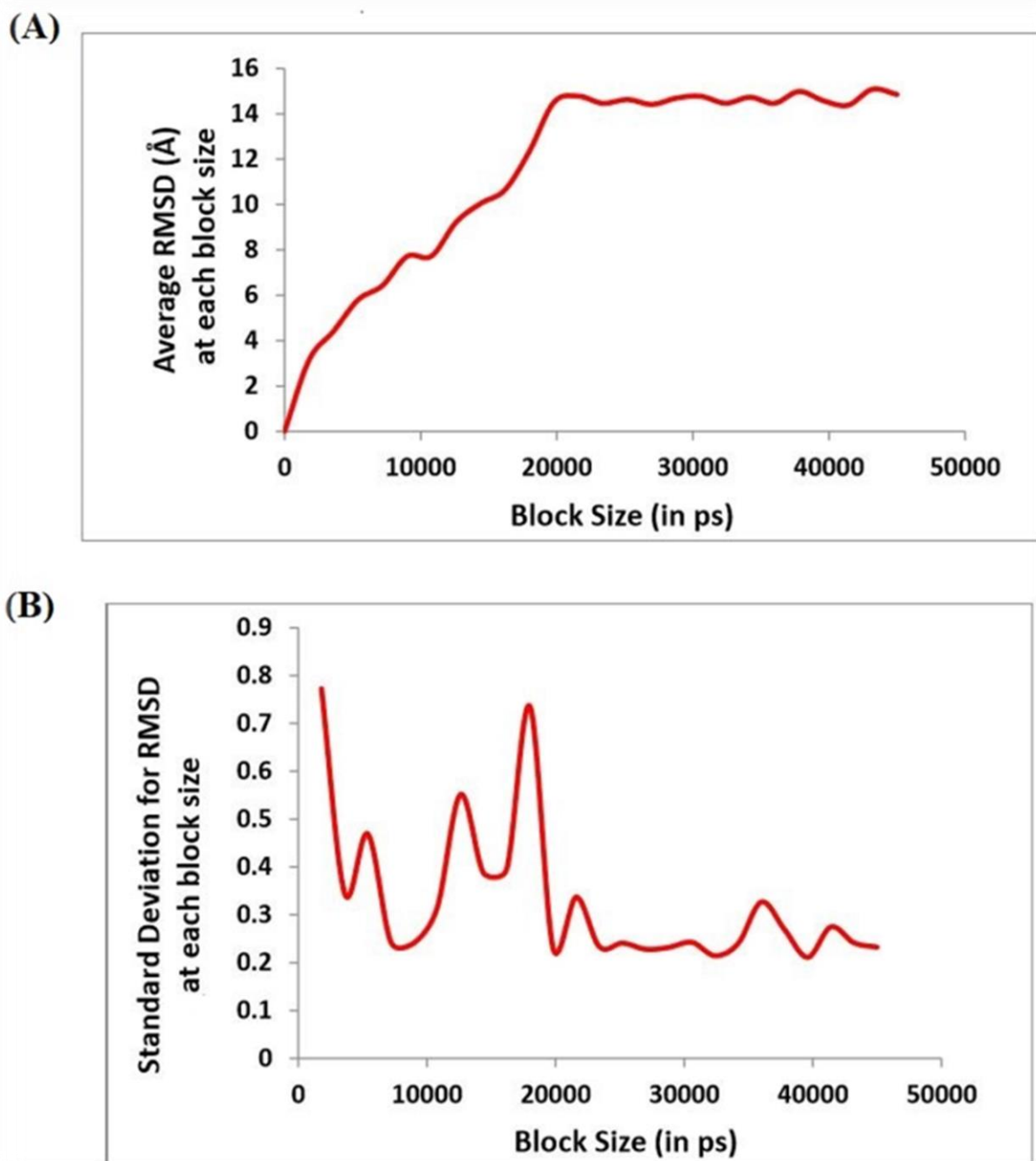
Figure 9.6. (A) Average RMSD at each block versus block size in picoseconds, (B) Standard deviation for the RMSD at each block size versus block size in picoseconds for the (α-Synuclein + OleA) complex Molecular dynamics trajectory

9.4.2. Analysis of the conformational changes observed during different intervals of simulation period:

The conformational changes observed in the apo and complex structures have been shown at different intervals of the simulation period (**Figure 9.7**). From **Figure 9.4(A)** and **Figure 9.7(A)**, it can be seen that αS structure in apo form is stabilized because of partial folding in the structure. In the complex, it is observed that the ligand

OleA binds to Leu 38, Tyr 39, Val 40, Lys 43 residues present in the N-terminal domain of αS (as shown in **Figure 9.8**). And with the residue Val 40, OleAis noticed to form hydrogen bond. All these interactions have been depicted using the LigPlot$^+$ software v.1.4.5 [504] in the **Table 9.2**.

From the snapshots depicted in **Figures 9.7(A) and 9.7(B)**, we observed that the secondary structure in the N-terminal and NAC domain of αS changes rapidly in the apo form, while in the complex form, the first helical portion till residues aa38 of monomeric αS do not undergo much change in secondary structure but the second helical portion that is present after residue index 43-44 show subtle changes in secondary structure as a function of simulation time. This is in agreement with one of the recent study [678, 679]. OleA is therefore seen to stabilize the αS monomeric structure by holding the helical secondary structure in the N-terminal and NAC domain. So the conformation of αS monomer is different in apo state and in the complex form with OleA. A recent study reported that the N-terminal of αS adopts a continuously helical conformation with a single break at residues 43-44, corresponding to the boundary between the first and second coding exons [679]. This particular "hinge" has been reported to be necessary to allow αS binding to lipid surfaces of different curvature [679]. In another study, a noticeable break in the helical pattern was observed around residues 43 and 44, revealing an interruption of the helical structure in this region [678]. We also observed similar characteristic secondary structural features that involve the continuous helical conformation in the N-terminal and NAC domain of (α-Synuclein + OleA) complex with a single break at residues 43-44. We have performed two other additional MD simulations (simulation-II and III) to confirm the characteristic dynamic behavior of α-Synuclein (apo) and (α-Synuclein + OleA) complex. The snapshots of the conformers of α-Synuclein (apo) and (α-Synuclein + OleA) complex recorded from the two simulations have been shown in **Figures 9.9 and 9.10**. We noticed the secondary structure profile for α-Synuclein (apo) and (α-Synuclein + OleA) complex follows the same trend as we observed in the first simulation (**Figures 9.7(A) and (B)**).
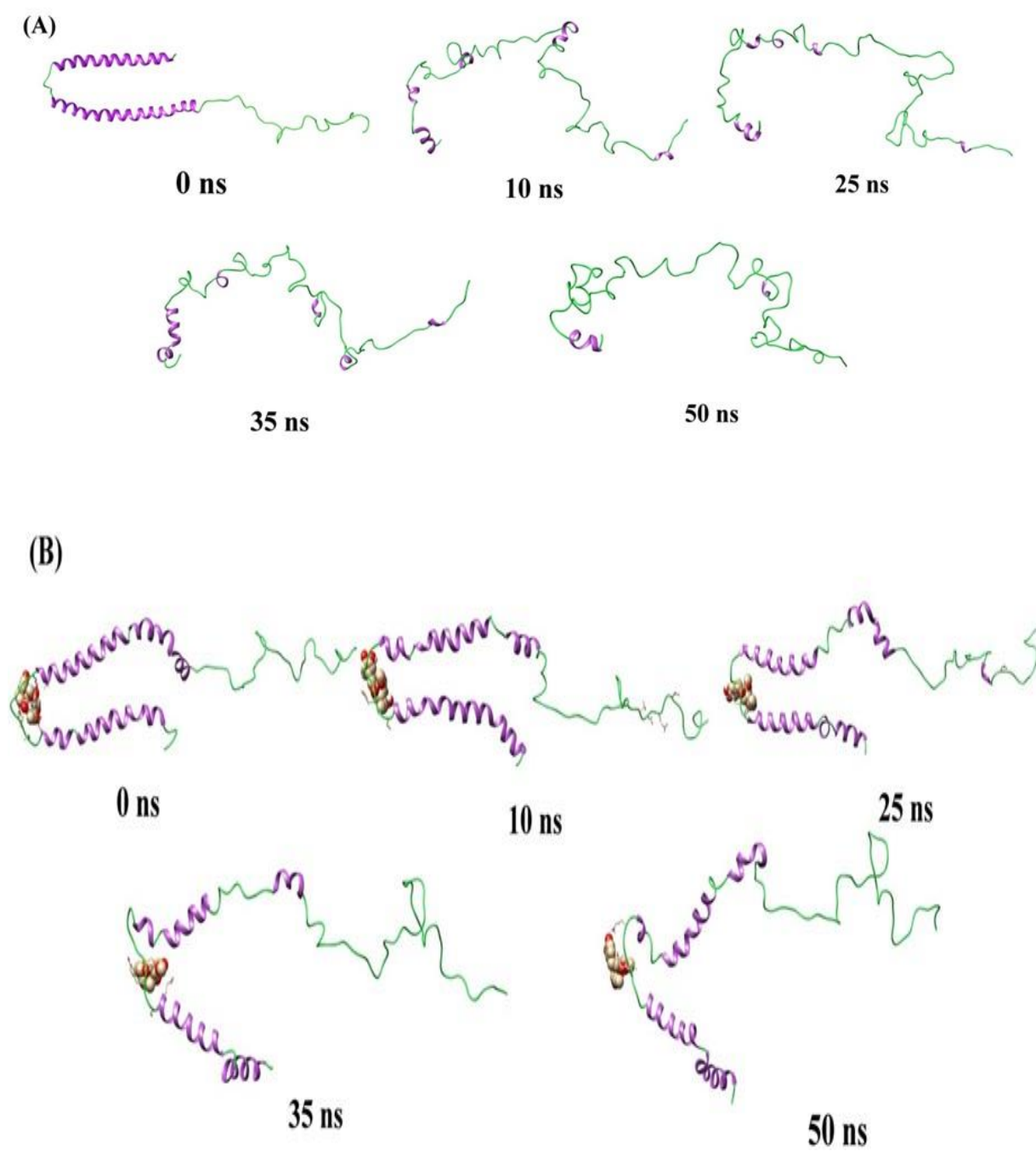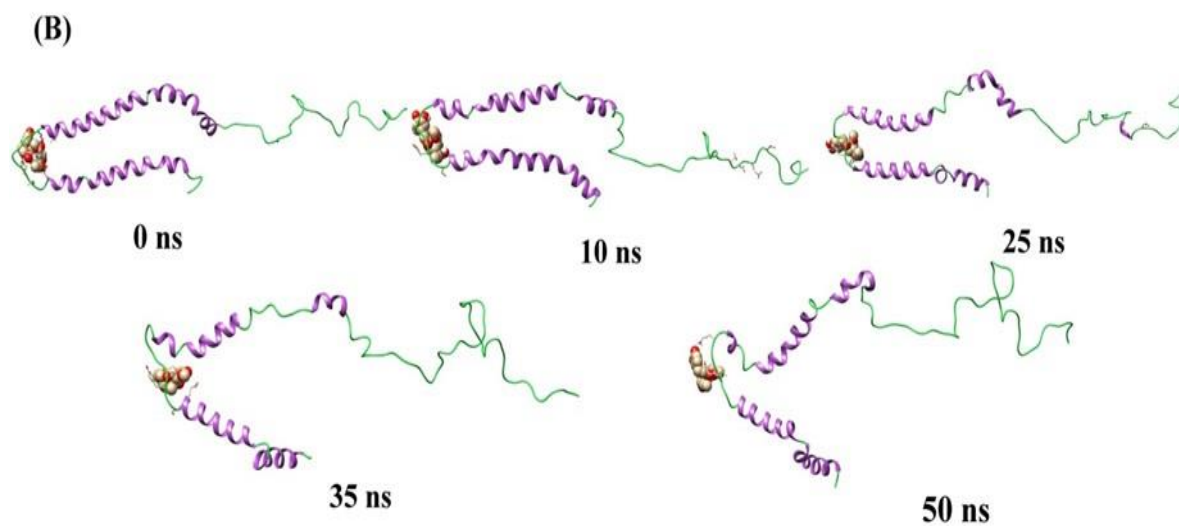
Figure 9.7. Snapshots of the conformers of α-Synuclein taken at different interval of simulation time (A) α-Synuclein (apo), (B) (α-Synuclein + OleA) complex.
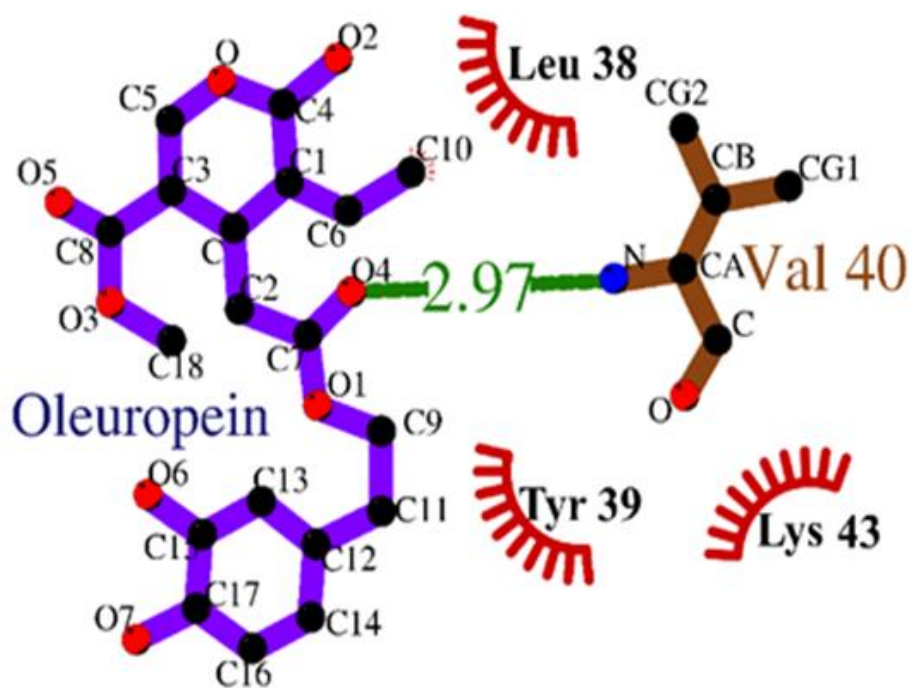
Figure 9.8. *Ligplot analysis showing the interaction of hydrophobic residues of α-Synuclein with OleA.*

(B)
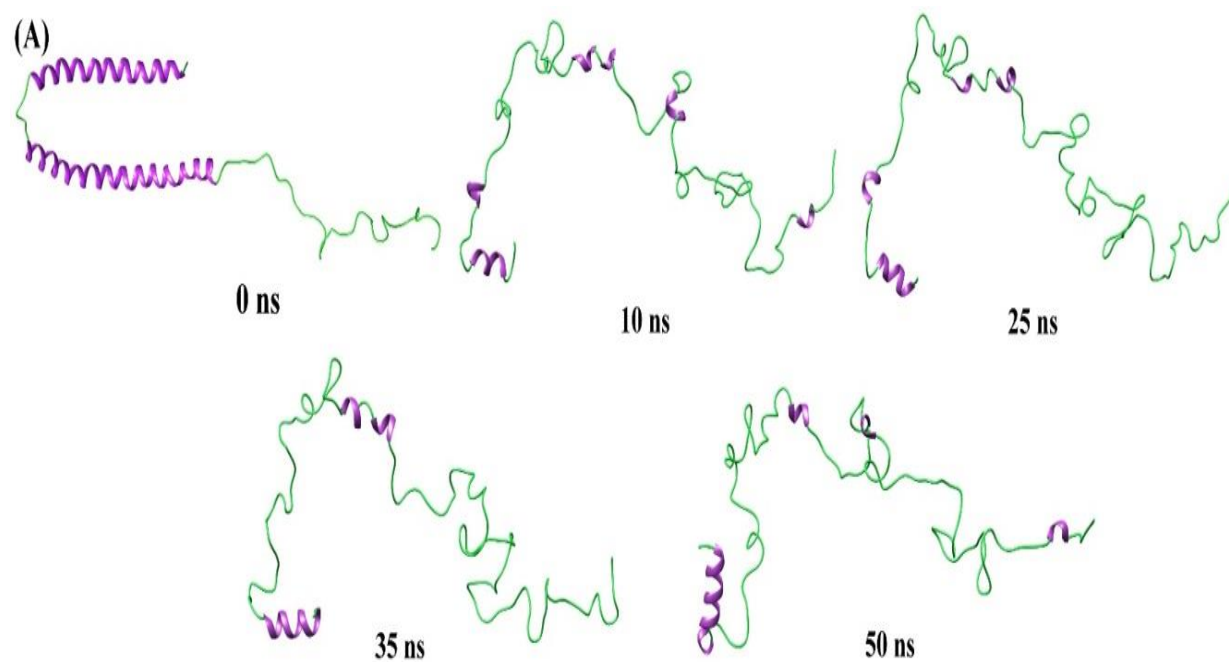
Figure 9.9. Snapshots of the conformers (from simulation-II) of α-Synuclein taken at different interval of simulation time (A) α-Synuclein (apo), (B) (α-Synuclein + OleA) complex.

(A)

(B)

Figure 9.10. Snapshots of the conformers (from simulation-III) of α-Synuclein taken at different interval of simulation time (A) α-Synuclein (apo), (B) (α-Synuclein + OleA) complex.

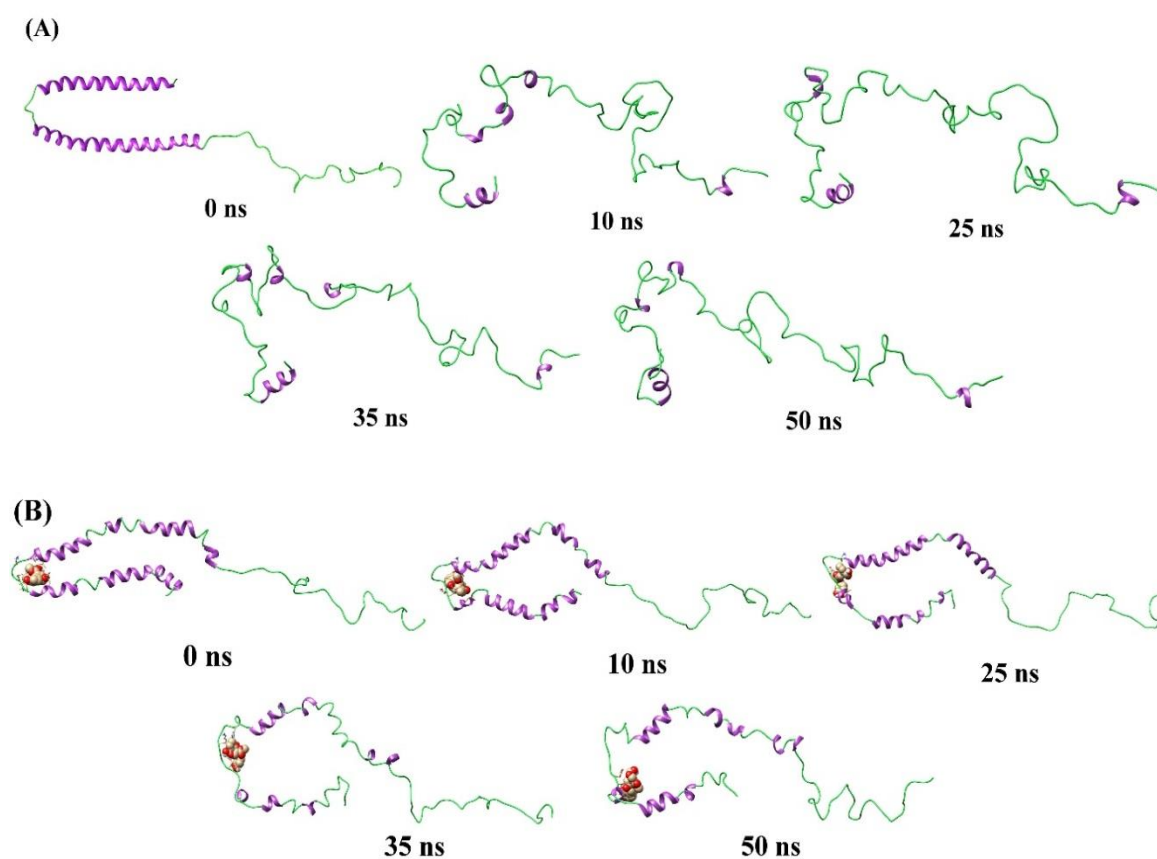*Table 9.2. Interactions of residues of α-Synuclein (receptor) with OleA (ligand) obtained from Ligplot⁺ software.*

α-Synuclein(Receptor)			< --->	OleA(ligand)			
Atom name	Residue name	Residue number		Atom name	Residue name	Residue number	Bond distance
CD2	TYR	40	< --->	O1	LIG	1	3.65
CE1	TYR	40	< --->	O1	LIG	1	3.80
CE2	TYR	40	< --->	O1	LIG	1	3.16
CZ	TYR	40	< --->	O1	LIG	1	3.32
OH	TYR	40	< --->	O1	LIG	1	3.76
CA	TYR	40	< --->	O4	LIG	1	3.37
C	TYR	40	< --- >	O4	LIG	1	3.63
CG	TYR	40	< --- >	O4	LIG	1	3.54
CD2	TYR	40	< --- >	O4	LIG	1	3.58
N	VAL	41	< --- >	O4	LIG	1	2.97
CA	TYR	41	< --- >	O4	LIG	1	3.83
C	TYR	40	< --->	O1	LIG	1	3.83
O	TYR	40	< --->	O1	LIG	1	3.67
CG2	TYR	40	< --->	O1	LIG	1	3.79
O	TYR	40	< --->	C2	LIG	1	3.66
CG	TYR	40	< --->	C2	LIG	1	3.89
CD1	TYR	40	< --->	C2	LIG	1	3.42
CE1	TYR	40	< --- >	C2	LIG	1	3.39
CZ	TYR	40	< --- >	C2	LIG	1	3.82
CG	TYR	40	< --- >	C7	LIG	1	3.52
CD1	TYR	40	< --- >	C7	LIG	1	3.59
CE1	TYR	40	< --- >	C7	LIG	1	3.68
CE2	TYR	40	< --- >	C7	LIG	1	3.51
CZ	TYR	40	< --- >	C7	LIG	1	3.65
CE2	TYR	40	< --- >	C9	LIG	1	3.52
O	TYR	40	< --- >	C10	LIG	1	2.96
CE2	TYR	40	< --- >	C11	LIG	1	3.85
C	LYS	44	< --- >	C18	LIG	1	3.80
O	LYS	44	< --- >	C18	LIG	1	3.09

9.4.3. Secondary structure analysis:

The secondary structure analysis for α-Synuclein (apo) and (α-Synuclein + OleA) complex was carried out using the Kabsch and Sander algorithm [532] incorporated in their DSSP (Dictionary of Secondary Structure for Protein) program. The results for secondary structure analysis have been plotted in **Figures 9.11(A) and 9.11(B)**. The plot shows the secondary structure variation of each residue as a function of frame numbers. In the case of apo, we see rapid changes in the secondary structure in the N-terminal and NAC domain. While in the complex form of αS, the continuous helix in the N-terminal

and NAC domain is preserved, with the breakage in between residues aa43-44. We also quantified the probable secondary structure that can be adopted in the case of the apo and complex form of αS as a function of residue index (as shown in **Figure 9.11(C) and 9.11(D)**). From this plot, we observed the complex form of αS to have higher helical content than the apo form of αS. Besides, using YASARA software [625], we also calculated the percentage of individual secondary structure content in apo and complex forms of αS from their corresponding average structure obtained from 50 ns MD simulations. The results were summarized in **Table 9.3**. From **Table 9.3**, we see the complex form of αS to have higher helical content than the apo form. From this secondary structure analysis, it can be inferred that OleA stabilizes the monomeric form of αS by holding the continuous helical conformation in the N-terminal and NAC domain of αS.
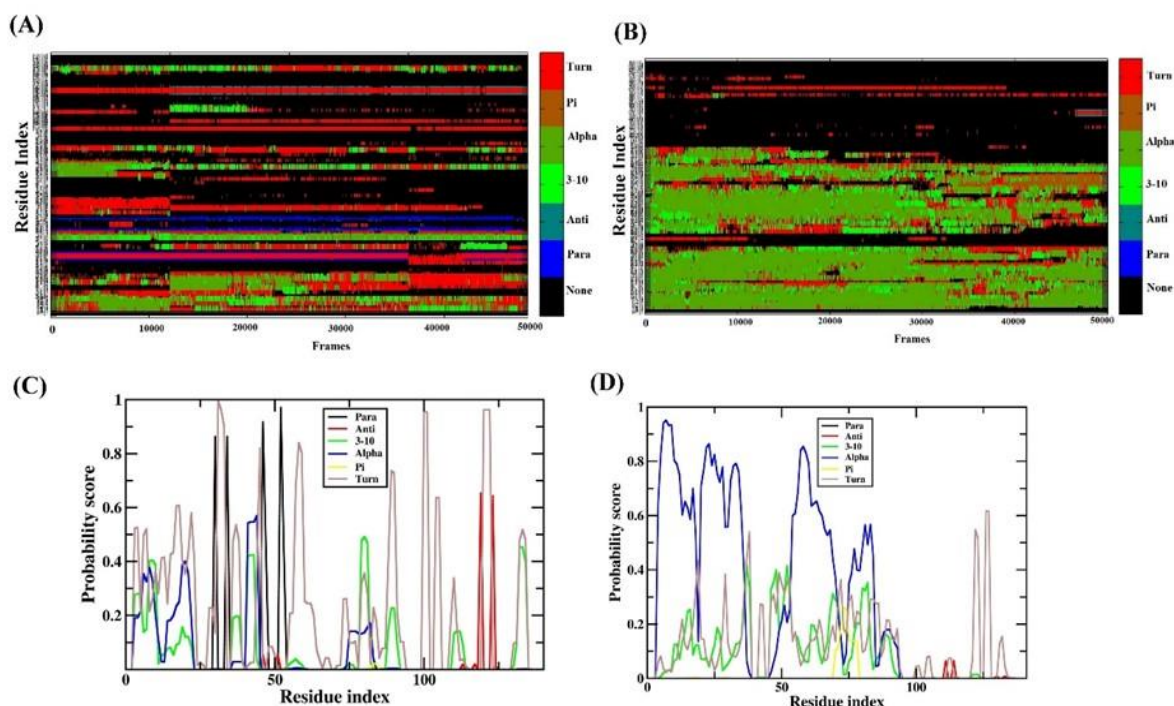
***Figure 9.11.*** *Secondary structure analysis of (A) α-Synuclein (apo), (B) (α-Synuclein + OleA) complex. Secondary structure Probability score of residue index for (C) α-Synuclein (apo), (D) (α-Synuclein + OleA) complex.*

Table 9.3. *Secondary structure content of the α-Synuclein (apo) and (α-Synuclein + OleA) complex showing the secondary contents of α-helix, β-sheets, Turns, 3_{10}-helix, Coils, and Pi.*

α-Synuclein Variants	Secondary Structure content					
	α-helix (%)	β-sheets (%)	Turns (%)	3_{10}-helix (%)	Coils (%)	Pi (%)
Apo	0	5.7	28.6	0	65.7	0
(α-Synuclein +OleA) complex	30	0	20	2.9	47.1	0

9.4.4. Hydrogen bond analysis:

We performed the hydrogen bond analysis for the overall structure of monomer αS in both the apo and complex forms as shown in **Figures 9.12(A) and 9.12(B)** respectively. To calculate the hydrogen bond, the cut-off for angle and distance was set to 120° and 3.5 Å respectively. We have found that there is no marked difference in the number of intramolecular hydrogen bonds between α-Synuclein (apo) and the (α-Synuclein + OleA) complex. We also investigated the intra-molecular hydrogen bond occupancy between the NAC and C-terminal region in both apo (**Table 9.4**) and complex form (**Table 9.5**) using their respective MD trajectory files. For the intra-molecular hydrogen bond analysis in the case of apo form, we have considered the residues aa61-95 for the NAC region and residues aa96-140 for the C-terminal region. In the case of complex form, we have considered the residues aa62-96 for the NAC region and residues aa97-141 for the C-terminal region. From **Figure 9.12(C) and 9.12(D)**, the average number of intra-molecular hydrogen bonds between NAC and C-terminal were found to be 3 in apo and 1 in case of the complex form of αS. This is so because the NAC and C-terminal regions are wider apart in the case of the complex form of αS than the apo form. The results were stipulated according to the occupancy, bond length, and the bond angle formed (HA–H–HD) between the hydrogen bond donor (HD) and acceptor (HA) atoms.
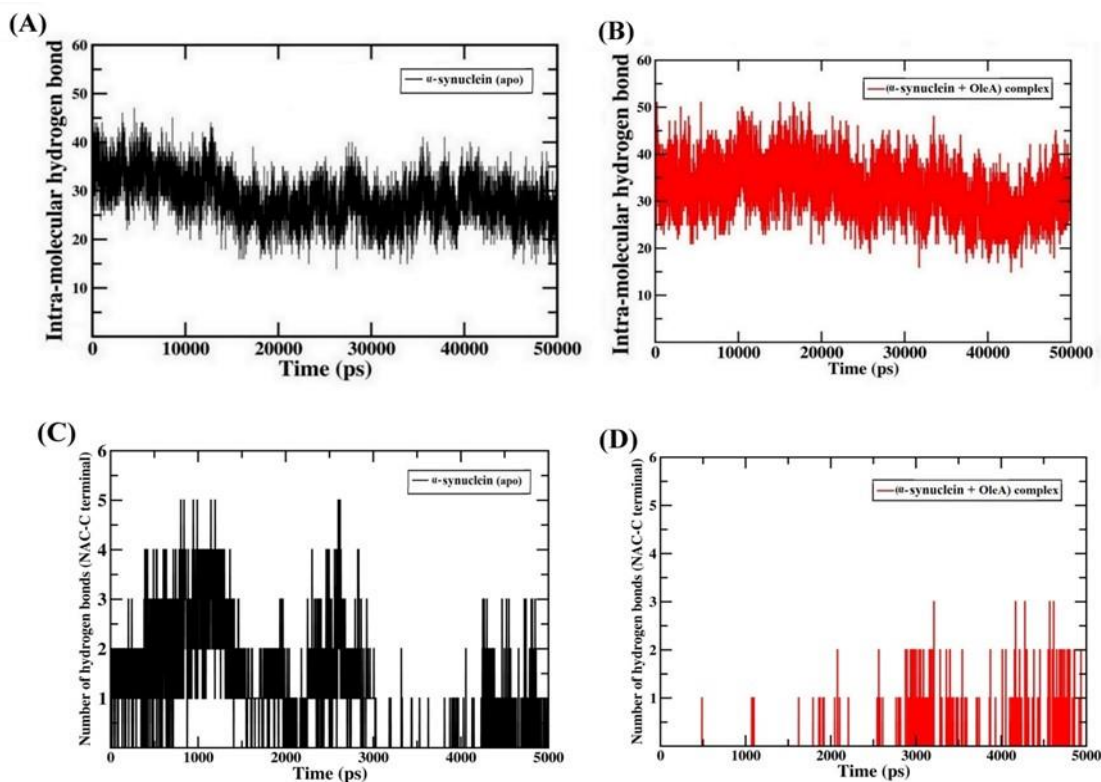
Figure 9.12. *The total number of intra-molecular hydrogen bonds present in whole structure for (A) α-Synuclein (apo), (B) (α-Synuclein + OleA) complex. The total number of intra-molecular hydrogen bonds between NAC and C-terminal domain in (C) α-Synuclein (apo), (D) (α-Synuclein + OleA) complex.*

Table 9.4. *Intra- molecular Hydrogen bond occupancy between NAC and C-terminal domain of α-Synuclein (apo).*

Acceptor	Donor	Fraction	Average Distance (Å)	Average Angle(º)
LYS_98@HG2	VAL_96@CB	0.0018	2.9256	139.8006
LYS_98@H	VAL_96@CB	0.0014	2.894	146.0744
LYS_97@HE3	PHE_95@CE2	0.0009	2.9101	146.5537
LYS_98@H	VAL_96@CG2	0.0009	2.9193	148.7936
GLN_100@HE21	VAL_96@CG2	0.0005	2.8565	143.1733
LYS_97@HG3	PHE_95@CE2	0.0004	2.9465	142.9428

LYS_98@H	VAL_96@CG2	0.0004	2.8978	142.1204
GLN_100@HE22	VAL_96@CG2	0.0004	2.8627	147.7553
LYS_97@HG3	PHE_95@CE1	0.0003	2.9669	140.9906
LYS_98@HE2	VAL_96@CG2	0.0003	2.9483	144.263
LYS_98@HE2	VAL_96@CG1	0.0003	2.8777	139.3384
ASP_99@HB2	VAL_96@CB	0.0003	2.9706	140.7942
GLN_100@HG3	PHE_95@CE2	0.0003	2.9164	139.2789
LYS_97@HG2	PHE_95@CE2	0.0002	2.9469	137.6289
LYS_97@HE2	PHE_95@CE1	0.0002	2.9581	150.7708
LYS_98@HE2	VAL_96@CG1	0.0002	2.8796	143.8116
GLN_100@HE22	VAL_96@CG1	0.0002	2.9376	143.6786
LYS_97@HB2	PHE_95@CE1	0.0001	2.9183	141.9421
LYS_97@HB2	PHE_95@CE2	0.0001	2.9904	141.6481
LYS_97@HG3	PHE_95@CD1	0.0001	2.9718	144.6032
LYS_97@HE2	PHE_95@CZ	0.0001	2.9362	140.0901
LYS_97@HE3	PHE_95@CE1	0.0001	2.9397	135.6953

Table 9.5. *Intra-molecular Hydrogen bond occupancy between NAC and C-terminal domain of (α-Synuclein + OleA) complex.*

Acceptor	Donor	Fraction	Average Distance (Å)	Average Angle(º)
GLU_105@OE2	SER_87@OG	0.179	2.6941	164.734
GLU_105@OE1	SER_87@N	0.1048	2.8667	158.75
GLU_104@OE2	SER_87@OG	0.0952	2.7018	164.754
GLU_104@OE1	SER_87@OG	0.0558	2.6918	163.688
GLU_105@OE1	SER_87@OG	0.044	2.7219	163.493
GLU_104@OE2	SER_87@N	0.015	2.8303	152.884
LYS_96@HE3	ALA_89@CB	0.0092	2.9177	151.355
LYS_96@HE3	ALA_89@CB	0.0034	2.9099	145.029
GLN_99@HE22	ALA_89@CB	0.0014	2.8935	142.496
LYS_96@HE3	ALA_89@CB	0.0012	2.8848	148.269
GLU_105@OE2	SER_87@N	0.0012	2.9551	142.979
LYS_96@HD3	ALA_89@CB	0.001	2.8931	139.063
LYS_96@HD3	ALA_89@CA	0.001	2.9396	141.174
LYS_96@HZ3	THR_75@CG2	0.001	2.8856	143.181
LYS_96@HE2	THR_92@CG2	0.0008	2.8692	154.939
LYS_96@HE2	THR_92@CG2	0.0008	2.9365	148.028
LYS_96@HZ3	THR_75@CG2	0.0006	2.924	139.655
GLN_99@HE21	ALA_89@CB	0.0006	2.8379	138.273
GLN_99@HE22	ALA_90@CA	0.0006	2.9409	149.404
LYS_96@HB2	ALA_89@CB	0.0004	2.9503	135.449
LYS_96@HB3	ALA_89@CB	0.0004	2.9771	141.74
LYS_96@HD2	ALA_89@CB	0.0004	2.9654	147.532
LYS_96@HD2	ALA_89@CB	0.0004	2.9523	150.409
GLU_104@HG3	ALA_89@CB	0.0004	2.936	135.334
GLU_105@CD	SER_87@OG	0.0004	2.9799	159.428

9.4.5. Analysis of the hydrophobic contacts:

The electrostatic and hydrophobic interactions are important to understand the intra-molecular contacts in αS. Therefore, we measured the hydrophobic intra-molecular contacts in the NAC domain of apo and complex form of αS (**Figure 9.13A**). We observed that the number of contacts within the NAC region remains almost the same in both apo and complex form of αS. We also investigated the hydrophobic interaction present in NAC and C-terminal domain of αS in apo and complex form (**Figure 9.13B**). The interaction between NAC and C-terminal region as determined by the number of contacts is observed to be relatively larger in the apo state than the complex state. This observation supports the strong intra-molecular interaction between NAC and C-terminal domain in apo form of αS than in the complex. These interactions in apo form of αS play a significant role and influence the early events of the fibrillation process and potential. In the case of complex, we see OleA stabilize the NAC and C-terminal regions of αS monomer, preventing the long-range hydrophobic interactions that favor amyloid aggregation.
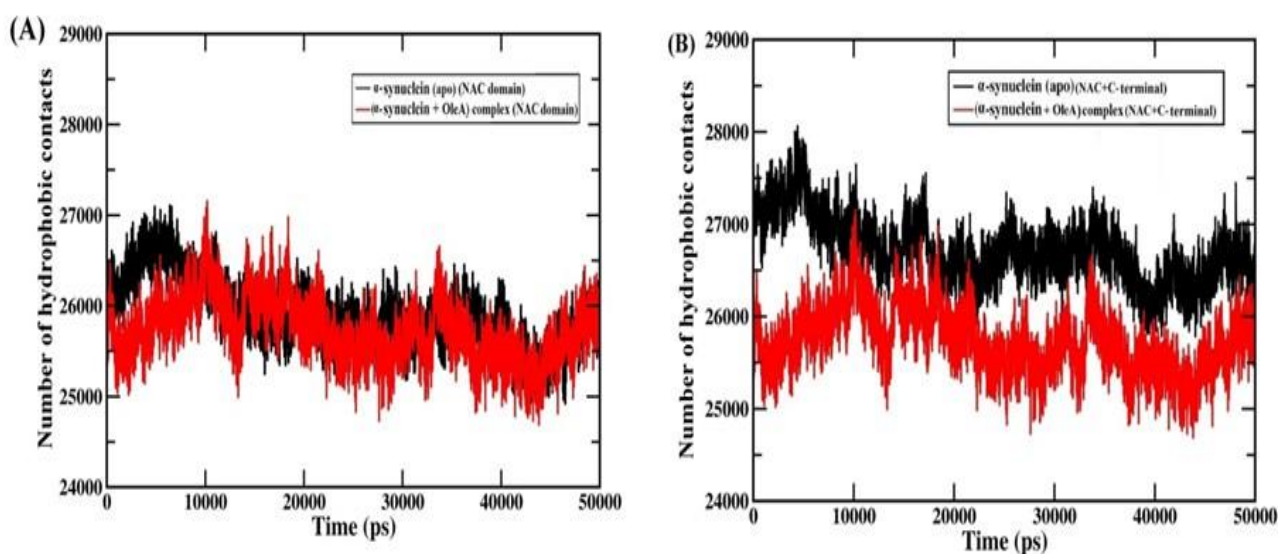

Figure 9.13. *(A) Long-range hydrophobic interactions in the NAC domain of α-Synuclein (apo) and (α-Synuclein + OleA) complex, (B) Long-range hydrophobic interactions between the NAC and C-terminal domain of α-Synuclein (apo) and (α-Synuclein + OleA) complex.*

9.4.6. Analysis of the distance between NAC and C-terminal domains for the two systems:

We also measured the center of mass distance between the NAC and C-terminal domains for the two systems: apo and the complex structure. The distance between the NAC region and C-terminal domains were measured as a function of simulation time using their respective trajectory files. From **Figure 9.14**, we can see that the distance between the NAC and C-terminal domains for the apo state is lower than the distance for the complex state. However, the distance between the NAC and C-terminal domains for the apo state is found to be more stable than the distance for the complex state. In the presence of OleA, the NAC and C-terminal domains in αS are placed wider apart and as a result the number of long-range interactions (that are critical for amyloid formation) between them is decreased.

Therefore, we see when OleA is in the binding pocket, it prevents the long-range hydrophobic interactions that lead to amyloid aggregation. We have reconfirmed this from the analysis of trajectories obtained from two other additional MD simulation runs (**Figures 9.15 and 9.16**). From **Figures 9.15 and 9.16**, we noticed the distance between the NAC and C-terminal domains for the apo state remains lower than the distance for the complex state.
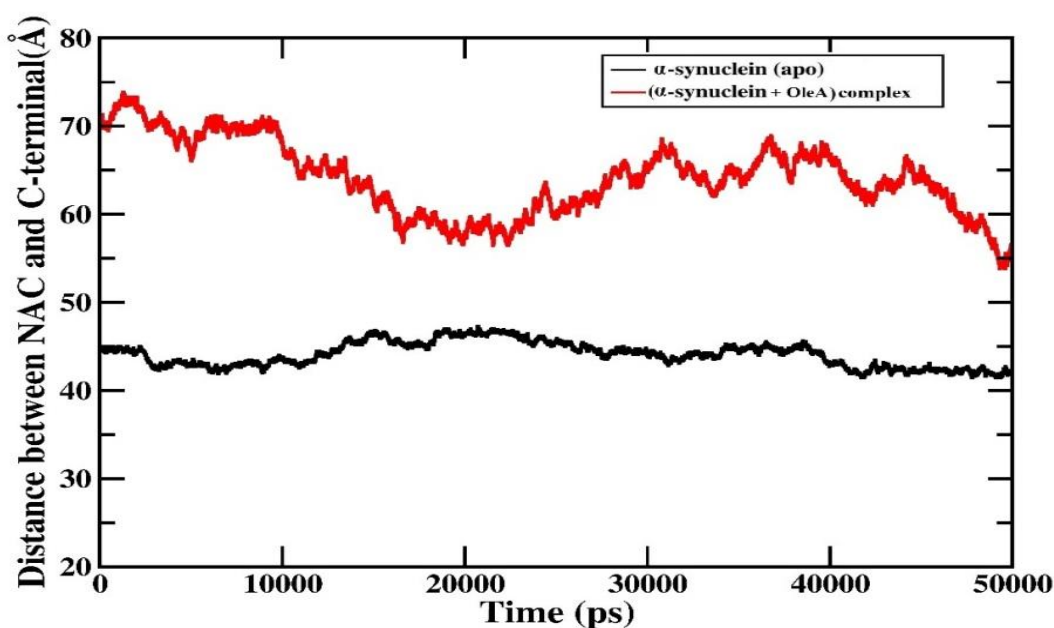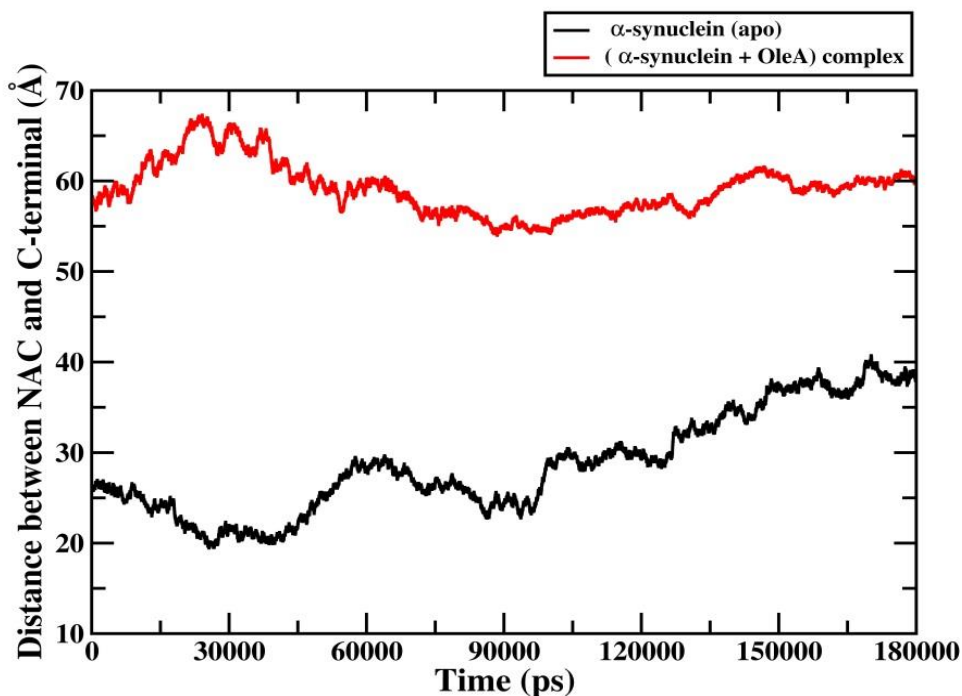
Figure 9.14. *Distance analysis between NAC and C-terminal domain of α-Synuclein with respect to time in the presence and absence of OleA.*
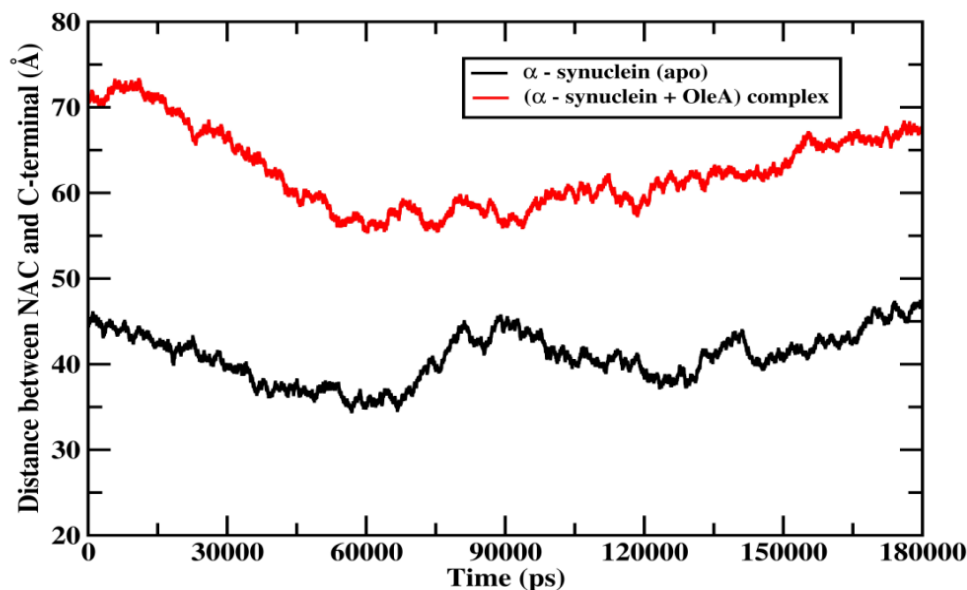
Figure 9.15.Intra-molecular distance analysis (from simulation-II) between NAC and C-terminal domains as a function of simulation time for the α-Synuclein (apo) and (α-Synuclein + OleA) complex.

Figure 9.16. Intra-molecular distance analysis (from simulation-III) between NAC and C-terminal domains as a function of simulation time for the α-Synuclein (apo) and (α-Synuclein + OleA) complex.

9.4.7. MM-PBSA and MM-GBSA calculations of (α-Synuclein + OleA) complex:

We performed binding free energy analysis on the (α-Synuclein + OleA) complex using the MM-PBSA/GBSA methods. These methods provide accurate results at a comparatively lower cost and gives information about the various contributions to the free energies such as the van der Waals, electrostatic and solvation energy. The entropy contribution to the binding free energy calculations were calculated using Normal Mode analysis [680]. The details of the BFE profile using MM-PBSA and MM-GBSA calculations have been summarized in **Table 9.6** and **Table 9.7** respectively. From **Table 9.6** and **9.7**, we observe the total binding free energy (ΔG_{bind}) to be -12.56 kcal mol^{-1} and -27.41 kcal mol^{-1} from MM-PBSA and MM-GBSA respectively. From the binding free energy values, we infer that OleA is strongly bound to the αS protein and thus the formation of this complex is favourable. The binding free energy analysis carried out for the trajectories obtained from two other additional MD simulation runs (simulation II and III) on the (α-Synuclein + OleA) complex reconfirms negative total binding free energy (-19.01/-2.91 kcal mol^{-1} from MM-GBSA/PBSA methods respectively (**Tables 9.8(A) and 9.8(B)**) and (-31.96 /-10.90 kcal mol^{-1} from MM-GBSA/PBSA methods respectively (**Table 9.9(A) and 9.9(B)**). The per-residue energy decomposition (PRED) is done to gain insight into the contribution of the individual active site amino acid residues and their interactions towards the overall ligand binding free energy. The PRED values were calculated using MM-PBSA/GBSA module of the AMBER 14 software package. The plots of binding free energy MM-PBSA/MM-GBSA calculation and PRED analysis have been shown in **Figures 9.17 and 9.18** respectively. The PRED analysis using MM-PBSA/GBSA algorithm showed that the binding affinity between the receptor-ligand is indeed high, and their intermolecular interaction can be credited to the residues **Leu 38, Tyr 39, Val 40, Lys 43** present in the N-terminal domain of αS.

Table 9.6. The various components of the Binding Free Energy (kcal mol^{-1}) calculated by Molecular Mechanics-Poisson−Boltzmann Surface Area (MM-PBSA) method for (α-Synuclein+OleA) complex.

Energy components	COMPLEX Energy (kcal mol^{-1})	LIGAND Energy (kcal mol^{-1})	RECEPTOR Energy (kcal mol^{-1})	DELTA Energy (kcal mol^{-1})
E_{vdw}	-624.23	-8.12	-593.77	-22.35
E_{ele}	-8682.16	12.23	-8679.36	-15.03
E_{PB}	-4543.60	-39.16	-4529.18	24.74
E_{SURF}	215.70	2.43	202.53	10.74
G_{gas}	-9306.39	4.11	-9273.12	-37.38
G_{solv}	-4327.90	-36.73	-4326.65	35.48
PB_{TOTAL}	**-13634.29**	**-32.62**	**-13599.77**	**-1.89**
TS_{TRA}	16.27	13.02	16.25	-12.99
TS_{ROT}	17.87	10.77	17.70	-10.61
TS_{VIB}	1667.02	31.43	1601.32	34.27
TS_{TOT}	**1701.16**	**55.22**	**1635.28**	**10.67**
ΔG_{bind}(kcal mol^{-1})				**-12.56**

*Abbreviations: Electrostatic energy (E_{ele}); van der Waals contribution (E_{vdw}); total gas phase energy (G_{gas}); nonpolar contribution to the solvation free energy (E_{SURF}); the electrostatic contribution to the solvation free energy (E_{PB}); sum of nonpolar and polar contributions to solvation (G_{solv}); final estimated binding free energy (PB_{TOTAL}); translational energy (TS_{TRA}); rotational energy (TS_{ROT}); vibrational energy (TS_{VIB}), total entropic contribution (TS_{TOT}); binding free energy (ΔG_{bind}).

Table 9.7. The various components of the Binding Free Energy (kcal mol^{-1}) calculated by Molecular Mechanics-Generalized−Borne Surface Area (MM-GBSA) method for (α-Synuclein+OleA) complex.

Energy components	COMPLEX Energy (kcal mol^{-1})	LIGAND Energy (kcal mol^{-1})	RECEPTOR Energy (kcal mol^{-1})	DELTA Energy (kcal mol^{-1})
E_{vdW}	-624.23	-8.12	-593.77	-22.35
E_{ele}	-8682.16	12.23	-8679.36	-15.03
E_{GB}	-4477.77	-36.91	-4464.66	23.79
E_{SURF}	103.65	3.57	103.25	-3.16
G_{gas}	-9306.39	4.11	-9273.12	-37.38
G_{solv}	-4374.12	-33.34	-4361.41	20.64
GB_{TOTAL}	-13680.51	-29.23	-13634.54	-16.74
TS_{TRA}	16.27	13.02	16.25	-12.99
TS_{ROT}	17.87	10.77	17.70	-10.61
TS_{VIB}	1667.02	31.43	1601.32	34.27
TS_{TOT}	1701.16	55.22	1635.28	10.67
ΔG_{bind}(kcal mol^{-1})				**-27.41**

*Abbreviations expanded under **Table 9.6.**

Table 9.8(A). The various components of the Binding Free Energy (kcal mol^{-1}) calculated by Molecular Mechanics-Generalized Borne Surface Area (MM-GBSA) method between (α-Synuclein+OleA) complex (for Simulation II).

Energy components	COMPLEX	LIGAND	RECEPTOR	DELTA
	Energy (kcal mol^{-1})	Energy (kcal mol^{-1})	Energy (kcal mol^{-1})	Energy (kcal mol^{-1})
E_{vdW}	664.61	-4.23	-635.98	-24.40
E_{ele}	-8984.29	1.36	-8950.26	-35.39
E_{GB}	-4160.73	-34.63	-4170.14	44.04
E_{SURF}	95.96	3.85	95.95	-3.83
G_{gas}	-9648.90	-2.87	-9586.24	-59.79
G_{solv}	-4064.76	-30.78	-4074.19	40.20
GB_{TOTAL}	-13713.67	-33.65	-13660.43	-19.59
TS_{TRA}	16.27	16.25	13.02	-12.99
TS_{ROT}	17.87	17.62	10.77	-10.53
TS_{VIB}	1647.97	1593.56	31.47	22.94
TS_{TOT}	1682.11	1627.43	55.26	-0.58
ΔG_{bind}(kcal mol^{-1})				**-19.01**

*Abbreviations expanded under **Table 9.6.**

Table 9.8(B). *The various components of the Binding Free Energy (kcal mol^{-1}) calculated by Molecular Mechanics-Poisson Boltzman Surface Area (MM-PBSA) method between (α-Synuclein+OleA) complex (for Simulation II).*

Energy components	COMPLEX	LIGAND	RECEPTOR	DELTA
	Energy (kcal mol^{-1})	Energy (kcal mol^{-1})	Energy (kcal mol^{-1})	Energy (kcal mol^{-1})
E_{vdW}	-664.61	-4.23	-635.98	-24.40
E_{ele}	-8984.29	1.36	-8950.26	-35.39
E_{PB}	-4213.35	-37.70	-4220.05	44.39
E_{SURF}	232.96	1.58	219.74	11.91
G_{gas}	-9648.90	-2.87	-9586.24	-59.79
G_{solv}	-3980.40	-36.13	-4000.58	56.30
PB_{TOTAL}	-13629.31	-38.99	-13586.82	-3.49
TS_{TRA}	16.27	16.25	13.02	-12.99
TS_{ROT}	17.87	17.62	10.77	-10.53
TS_{VIB}	1647.97	1593.56	31.47	22.94
TS_{TOT}	1682.11	1627.43	55.26	-0.58
ΔG_{bind}(kcal mol^{-1})				-2.91

*Abbreviations expanded under **Table 9.6.**

Table 9.9(A). *The various components of the Binding Free Energy (kcal mol^{-1}) calculated by Molecular Mechanics-Generalized Borne Surface Area (MM-GBSA) method between (α-Synuclein+OleA) complex (for Simulation III).*

| Energy components	COMPLEX	LIGAND	RECEPTOR	DELTA
	Energy (kcal mol^{-1})	Energy (kcal mol^{-1})	Energy (kcal mol^{-1}) ± SD	Energy (kcal mol^{-1}) ± SD
E_{vdW}	-675.67	-4.83	-643.08	-27.76
E_{ele}	-8887.38	1.39	-8867.49	-21.29
E_{GB}	-4267.36	-34.38	-4264.44	31.46
E_{SURF}	95.53	3.84	95.90	-4.22
G_{gas}	-9563.05	-3.43	-9510.57	-49.05
G_{solv}	-4171.83	-30.54	-4168.54	27.25
GB_{TOTAL}	-13734.88	-33.97	-13679.11	-21.79
TS_{TRA}	16.27	13.02	16.25	-12.99
TS_{ROT}	17.88	10.77	17.67	-10.56
TS_{VIB}	1668.37	31.43	1603.22	33.72
TS_{TOT}	1702.53	55.22	1637.14	10.17
ΔG_{bind}(kcal mol^{-1})				**-31.96**

*Abbreviations expanded under **Table 9.6.**

Table 9.9(B). The various components of the Binding Free Energy (kcal mol⁻¹) calculated by Molecular Mechanics-Poisson Boltzmann Surface Area (MM-PBSA) method between (α-Synuclein+OleA) complex (for Simulation III).

| Energy components	COMPLEX Energy (kcal mol⁻¹)	LIGAND Energy (kcal mol⁻¹)	RECEPTOR Energy (kcal mol⁻¹)	DELTA Energy (kcal mol⁻¹)
E_{vdW}	-675.67	-4.83	-643.08	-27.76
E_{ele}	-8887.38	1.39	-8867.49	-21.29
E_{PB}	-4328.55	-36.73	-4326.53	34.71
E_{SURF}	237.88	1.51	222.76	13.46
G_{gas}	-9563.05	-3.43	-9510.57	-49.05
G_{solv}	-4090.67	-35.23	-4103.77	48.32
PB_{TOTAL}	13653.73	-38.66	-13614.34	-0.73
TS_{TRA}	16.27	13.02	16.25	-12.99
TS_{ROT}	17.88	10.77	17.67	-10.56
TS_{VIB}	1668.37	31.43	1603.22	33.72
TS_{TOT}	1702.53	55.22	1637.14	10.17
ΔG_{bind}(kcal mol⁻¹)				**-10.90**

*Abbreviations expanded under **Table 9.6.**
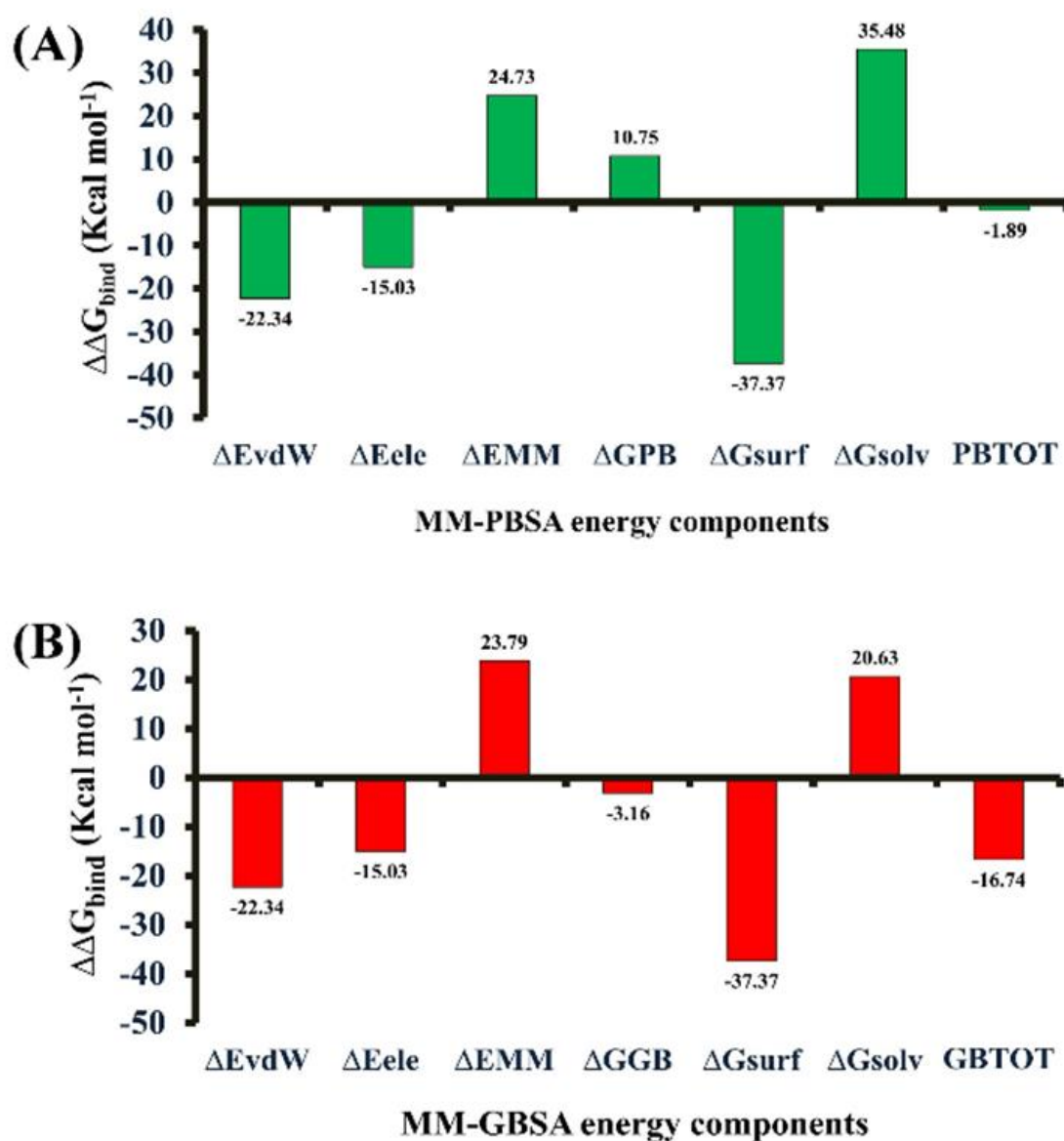
Figure 9.17. *ΔΔG_bind of various energy components in (A) MM-PBSA and (B) MM-GBSA method of Binding free energy calculation of (α-Synuclein + OleA) complex.*

Figure 9.18.Per-residue energy decomposition (PRED) plots for the interface residues of ligand (OleA) and receptor α-Synuclein calculated by MM-GBSA/PBSA method.
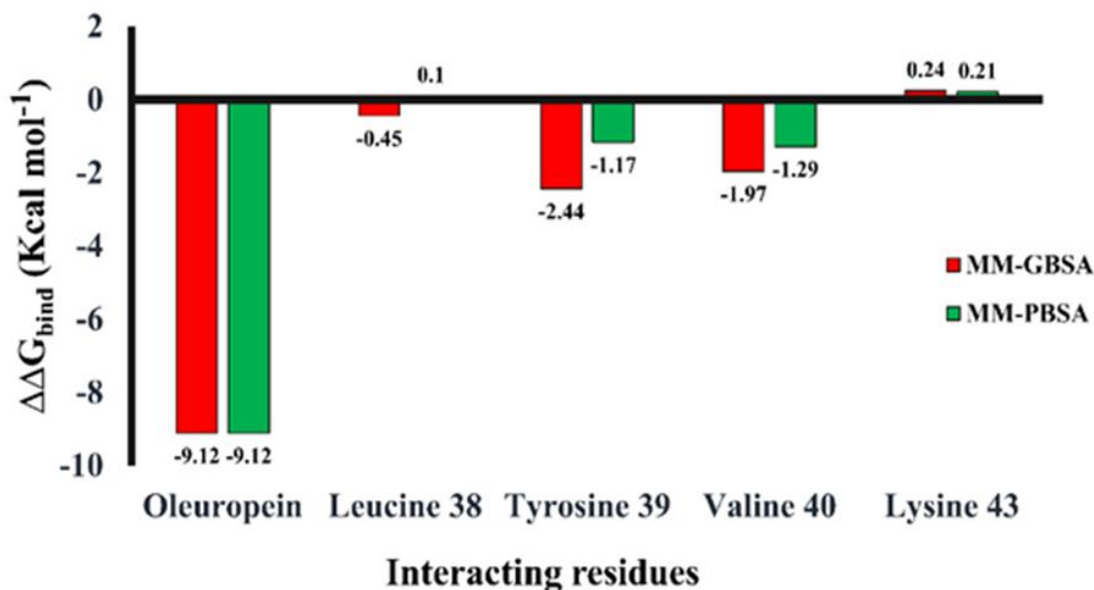
9.5. Conclusion:

In this study, an attempt has been made to understand the effect of OleA on the conformational dynamics and the aggregation propensity of αS monomer by carrying out molecular dynamics simulations on α-Synuclein (apo) and (α-Synuclein + OleA) complex using the AMBER force field. MD simulation results demonstrate that in the (α-Synuclein + OleA) complex, the continuous helix is preserved in the N-terminal region and NAC domain of αS with the breakage in between residues aa43-44. In addition, the intra-molecular distance between the NAC and C-terminal domains of αS is increased when OleA is tightly bound to αS. The molecular docking, binding free energy and per residue energy decomposition analysis using MM-PBSA/GBSA methods highlighted that the OleA is strongly bound to the αS monomer. From the contact analysis, we noticed relatively a lesser number of long-range hydrophobic interactions (that plays critical role in amyloid formation) between the NAC and C-terminal domains in the (α-Synuclein + OleA) complex than in α-Synuclein (apo). We have found that there is no marked difference in the number of intra-molecular hydrogen bonds between the α-Synuclein (apo) and the (α-Synuclein + OleA) complex. Since the NAC and C-terminal regions are wider apart and stable in the complex, the average number of intra-molecular hydrogen bonds was found to be more in apo than in complex. In summary, this work helps us in understanding the role of OleA in stabilizing the monomeric structure of αS resulting in the conformation that favors the growth of stable and non-toxic aggregates.